



Electrochemical Sensor Based on Reduced Graphene Oxide/Double-Walled Carbon Nanotubes/Octahedral Fe₃O₄/Chitosan Composite for Glyphosate Detection

Cao Thi Thanh¹ · Nguyen Hai Binh¹ · Phan Nguyen Duc Duoc^{2,3} · Vu Thi Thu⁴ · Pham Van Trinh¹ · Nguyen Ngoc Anh¹ · Nguyen Van Tu¹ · Nguyen Viet Tuyen⁵ · Nguyen Van Quynh⁴ · Vu Cam Tu⁴ · Bui Thi Phuong Thao⁶ · Pham Duc Thang² · Hiroya Abe⁷ · Nguyen Van Chuc^{1,8}

Received: 13 December 2020 / Accepted: 8 March 2021 / Published online: 20 March 2021
© The Author(s), under exclusive licence to Springer Science+Business Media, LLC, part of Springer Nature 2021

Abstract

In this work, reduced graphene oxide/double-walled carbon nanotubes/octahedral-Fe₃O₄/chitosan composite material modified screen-printed gold electrodes (rGO/DWCNTs/Oct-Fe₃O₄/Cs/SPAuE) under inhibition of urease enzyme was developed for the determination of glyphosate (GLY). The electrochemical behaviors of GLY on these electrodes were evaluated by square wave voltammetry (SWV). With the electroactive surface area is 1.7 times higher than that of bare SPAuE, the rGO/DWCNTs/Oct-Fe₃O₄/Cs/SPAuE for detection of GLY shows a low detection limit (LOD) of ~0.08 ppb in a large concentration range of 0.1–1000 ppb. Moreover, it is also successfully applied to the determination of GLY in river water samples with recoveries and relative standard deviations (RSDs) from 98.7% to 106.9% and from 0.79% to 0.87%, respectively. The developed composite will probably provide an universal electrochemical sensing platform that is very promising for environmental monitoring.

Keywords Electrochemical sensor · Glyphosate · Reduced graphene oxide · Double-walled carbon nanotube · Octahedral Fe₃O₄ · Chitosan

Glyphosate (GLY) is one of the most commonly used herbicides worldwide (Turhan et al. 2020) and its residue in water, soil has posed serious problems on human health and ecological balance (Chen et al. 2019). Conventional methods to detect GLY include ultra-high performance liquid chromatography coupled with mass spectrometry (UHPLC-MS/

MS) (Zhang et al. 2020), gas chromatography (Motojyuku et al. 2008), and capillary electrophoresis (Wei et al. 2013). Typically, these methods require highly-skilled operators, expensive instruments, and complicated sample treatment. To overcome aforementioned issues, electrochemical sensors have been introduced for in-situ detection of GLY at

✉ Hiroya Abe
h-abe@jwri.osaka-u.ac.jp

✉ Nguyen Van Chuc
chucnv@ims.vast.vn

¹ Institute of Materials Science, Vietnam Academy of Science and Technology, 18 Hoang Quoc Viet, Cau Giay, Hanoi, Vietnam

² VNU-University of Engineering and Technology, 144 Xuan Thuy, Cau Giay, Hanoi, Vietnam

³ Department of Physics, Nha Trang University, 02 Nguyen Dinh Chieu, Nha Trang, Vietnam

⁴ University of Science and Technology of Hanoi, Vietnam Academy of Science and Technology, 18 Hoang Quoc Viet, Cau Giay, Hanoi, Vietnam

⁵ Faculty of Physics, VNU University of Science, Vietnam National University, Hanoi, 334 Nguyen Trai, Thanh Xuan, Hanoi, Vietnam

⁶ Viet Tri University of Industry, Lam Thao, Viet Tri, Phu Tho, Vietnam

⁷ Joining and Welding Research Institute, Osaka University, 11-1 Mihogaoka, Ibaraki, Osaka 567-0047, Japan

⁸ Graduate University of Science and Technology, Vietnam Academy of Science and Technology, 18 Hoang Quoc Viet, Cau Giay, Hanoi, Vietnam

low cost and facile operation (Vaghela et al. 2018; Sok and Fragoso 2019).

With large specific surface area and high electrical conductivity, both carbon nanotubes (CNTs) and reduced graphene oxide (rGO) are considered to be promising electrode materials for electrochemical sensors (Gholivand et al. 2018; Setznagl and Cesarino 2020). The combination of CNTs and rGO will provide an interconnected carbonaceous structure which is very beneficial to improve electrochemical responses (Ghalkhani et al. 2020). To further enhance the sensitivity in the electrochemical sensors, the electrodes have currently been modified by combining rGO/CNTs with metal oxide particles such as iron oxide (Fe_3O_4) (Nehru et al. 2020), cerium oxide (CeO_2) (Sakthivel et al. 2019), cobalt oxide (Co_3O_4) (Kumar et al. 2015; Zhao et al. 2019) etc. Among these metal oxide materials, Fe_3O_4 is one of the most promising ones due to its low-cost, easy preparation, low toxicity, and good bio-compatibility. Especially, it was known that octahedral Fe_3O_4 (Oct- Fe_3O_4) particles exhibit excellent catalytic activity that might help to improve electrochemical responses (Dağcı Kıranşan et al. 2018; Kumar et al. 2018). However, the poor electrical conductivity and the agglomeration of Fe_3O_4 particles have restricted their applications in electrochemical sensors. Indeed, chitosan (Cs) owns excellent adhesivity, hydrophilicity, doping feasibility, availability of reactive hydroxyl and amine functional groups for chemical modifications. Therefore, the use of Cs as binding agent in preparation of rGO/CNTs- Fe_3O_4 is expected to limit the aggregation of nanoparticles and improved sensing performances. Comparing with single-walled carbon nanotubes (SWCNTs) and multiwalled-carbon nanotubes (MWCNTs), the outer wall of double-walled carbon nanotubes (DWCNTs) can be functionalized without changing the mechanical, thermal, electronic, and chemical stability, as well as isolation from the environment of the inner tube (Neves et al. 2012; Duoc et al. 2020). To the best of our knowledge, electrochemical determination of GLY by using a combination of rGO/DWCNTs, Oct- Fe_3O_4 and Cs (rGO/DWCNTs/Oct- Fe_3O_4 /Cs) composite modified electrode has not been reported.

Herein, the working electrode (WE) surface of the screen printed gold electrodes (SPAuE) was firstly covered by the rGO/DWCNTs/Oct- Fe_3O_4 /Cs composite material and was then covered by the urease. The urease/rGO/DWCNTs/Oct- Fe_3O_4 /Cs/SPAuE sensor was utilized as a useful tool for the determination of GLY using square wave voltammetry (SWV) technique.

Materials and Methods

Urease enzyme (EC 3.5.1.5, 42 U/mg) was purchased from Merck. Phosphate buffered saline (PBS, pH 7.0), glutaraldehyde (GA) and GLY were obtained from Sigma- Aldrich

(USA). Cs was purchased from Tokyo Chemical Co. Ltd. SPAuE-model DRP-C223AT with three electronic contacts for gold (Au, $d=1.6$ mm) as working electrode, Au as counter electrode and silver/silver chloride (Ag/AgCl) as a reference electrode were obtained from Dropsens, Spain.

Graphene oxide (GO) was synthesized from natural graphite powder by a modified Hummers method (Hummers and Offeman 1958). First, 1.0 g of graphite flakes and 1.0 g of potassium permanganate (KMnO_4) were mixed in 35 mL of sulfuric acid (H_2SO_4) solution under stirring at 50°C overnight. To remove excess KMnO_4 , the reaction mixture was diluted with 300 mL of deionized water and 25 mL of hydrogen peroxide (H_2O_2). Next, the solution was washed with 10% hydrochloric acid (HCl) and treated with ultrasonication for 1 h. Finally, GO suspension with concentration of 1 mg/mL was obtained after centrifugation at 4000 rpm for 40 min. DWCNTs were synthesized by chemical vapor deposition (CVD) technique and functionalized with $-\text{COOH}$ group as described in our previously published work (Duoc et al. 2020). Oct- Fe_3O_4 microparticles were synthesized by polyol method via the reduction of $\alpha\text{-FeOOH}$ solid precursors in ethylene glycol (EG) containing 12 vol.% water at 200°C for 48 h as described in our previously published work (Abe et al. 2019).

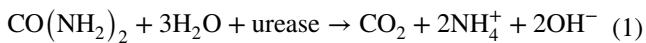
SPAuEs were first rinsed in ethanol, deionized water, and then dried by air gun. GO/DWCNTs nanohybrid structure was prepared by mixing GO and DWCNTs suspensions at the same concentrations (0.5 mg/mL) with the aid of ultrasonication for 30 min. Oct- Fe_3O_4 was ultrasonicated in 100 mL acetic acid (CH_3COOH 1%) solution containing 0.2 g Cs for 1 h, then centrifuged at 4000 rpm for 40 min to remove unbound Cs. After that, a fresh mixture (GO/DWCNTs/Oct- Fe_3O_4 /Cs) containing carbonaceous materials and oxide particles was prepared at volume ratio of 1:10 with the assistance of ultrasonication for 1 h. Then, 1 μL GO/DWCNTs/Oct- Fe_3O_4 /Cs homogenous suspension was pipetted onto the working electrode (WE), and left to be dried at 60°C for 1 h at atmospheric pressure in argon (Ar) gas in order to improve cross-linking between individual components and remove the solvents. Finally, GO/DWCNTs/Cs modified SPAuE (GO/DWCNTs/Cs/SPAuE) was electrochemically reduced in a 0.1 M PBS to gain reduced GO/DWCNTs/Cs/SPAuE (rGO/DWCNTs/Cs/SPAuE). For comparison, Oct- Fe_3O_4 /Cs modified SPAuE (Oct- Fe_3O_4 /Cs/SPAuE) and rGO/DWCNTs/Cs modified SPAuE (rGO/DWCNTs/Cs/SPAuE) were also prepared by the similar process.

0.5 μL urease enzyme solution (1 mg/10 μL) was immobilized onto rGO/DWCNTs/Oct- Fe_3O_4 /Cs/SPAuE with the aid of glutaraldehyde (GA) in ambient conditions for 12 h. The as-prepared sensors were stored in fridge at 4°C until use.

The surface morphology of the GO, DWCNTs, Oct- Fe_3O_4 and GO/DWCNTs/Oct- Fe_3O_4 /Cs hybrid samples was

investigated by field emission scanning electron microscopy (FESEM, Hitachi S-4800), transmission electron microscopy (TEM, JEM 2100), and atomic force microscopy (AFM, XE-100 Park Systems). The crystallinity of the samples was determined using a LabRAM HR800 (Horiba Jobin–Yvon) Raman spectroscopy in the range 1000–2500 cm^{-1} with 632.8 nm excitation source. The functional groups of the samples were measured by Fourier transform infrared spectra (FTIR, Nexus 670 Nicolet spectrometer). All electrochemical measurements were carried out with PamSens4 (Netherlands). Electrochemical behaviors of electrodes were tested by recording cyclic voltammograms over the potentials ranging between -200 and $+650$ mV at a scan rate of 50 mV/s in 2 mM $[\text{Fe}(\text{CN})_6]^{3-/4-}$ solution. The sensing performances of developed sensor were examined using SWV technique.

The working principle of as-prepared GLY sensors in this work is based on the inhibition of the GLY compound toward urease in the hydrolysis reaction:



It was known that GLY ($\text{OH}_2\text{-PO-NH-COOH}$) having P=O bond which might interact with nickel ion active center of urease to inhibit the catalytic activity of this enzyme. This allows GLY to act as a substrate-like inhibitor that reduces the binding of urea to urease, leading to inhibition of urease enzymatic activity (Vaghela et al. 2018). The sensing performances of GLY sensors were recorded using SWV method in presence of urea (30 mM) after being incubated in GLY solution for 10 min. SWV measurements were recorded at frequency of 50 Hz, start potential of -200 mV, end potential of $+650$ mV, step of 10 mV, scan rate of 50 mV/s, and amplitude of 20 mV. The relative inhibition degree (RI) was determined as follows: $\text{RI}(\%) = (I_0 - I_i)/I_0 \times 100$, where I_0 is the current response in the absence of GLY, I_i is the current response obtained after incubation with GLY.

Water samples were collected from Red River, northern Vietnam, and close to Hanoi city. The grab composite water sample was taken at the water depth of 30 cm by using Niskin bottle, following the sampling method of ISO 5667-3:2018. The monitoring parameters of water quality (pH, EC, etc.) (Table S1(Supporting information)) were conducted in field, and then the samples stored at 4°C in polyethylene bottle (in dark) before being transferred to the laboratory for further analysis. These river water samples were spiked with GLY (0.1–100 ppb), and then analyzed by using developed sensor according to the above-described protocol.

Results and Discussion

The surface morphologies of the synthesized GO, DWCNTs, Oct- Fe_3O_4 and GO/DWCNTs/Oct- Fe_3O_4 /Cs hybrid are presented in Fig. 1. For Cs, a smooth homogeneous surface is observed by SEM (Fig. S1(Supporting information)). The size of GO sheets is about 100 nm to several μm (Fig. 1a), and their thickness is of 1.5 nm (Fig. 1e). Figure 1b shows the SEM image of DWCNT fibers. The average inner and outer diameters of DWCNTs are 1.0 and 1.8 nm, respectively (Fig. 1f). The diameter of Oct- Fe_3O_4 particles is about 1 μm (Fig. 1c). SEM image of GO/DWCNTs/Oct- Fe_3O_4 /Cs (Fig. 1d) shows clearly the presence of the three materials on a very rough surface. The contents of carbon and oxygen atoms in GO were evaluated by energy dispersive X-ray spectroscopy (EDS) (Fig. S2(Supporting information)) to be 67.47 wt% and 32.53 wt%, respectively. The phase purity and crystal structures of Oct- Fe_3O_4 particles were confirmed by X-ray diffraction (XRD) (Fig. S3(Supporting information)). The XRD patterns demonstrate eight characteristic peaks for Fe_3O_4 corresponding to (111), (220), (311), (222), (400), (422), (511) and (440) (Abe et al. 2019). The peaks are sharp, indicating good crystallinity of the Fe_3O_4 sample.

FTIR spectra of (a) GO, (b) DWCNTs, (c) Oct- Fe_3O_4 , (d) Cs and (e) GO/DWCNTs/Oct- Fe_3O_4 /Cs are shown in Fig. 2. FTIR spectrum of GO shows typical bands assigned to stretching vibrations of C=C (1636 cm^{-1}) and vibration modes of OH and/or COOH (3426 cm^{-1}) (Bera et al. 2017), unoxidized sp^2 C=C (2085 cm^{-1}) (Boikanyo et al. 2016), C–O–H (1438 cm^{-1}), C–O–C (1024 cm^{-1}) (Hussain and Das 2017). FTIR spectrum of DWCNTs represents stretching vibrations of C=C (1632 cm^{-1}), OH (3448 cm^{-1}) (Pham et al. 2017). FTIR spectrum of Fe_3O_4 reveals vibration modes of Fe–O bonds (583 cm^{-1}), C=O (1632 cm^{-1}) and OH (3448 cm^{-1}) (Hussain and Das 2017). FTIR spectrum of Cs exhibits vibration bands at 3441 cm^{-1} , 1632 cm^{-1} and 1442 cm^{-1} related to the stretching vibrations of –OH and –NH groups, –C=O group and –NH bending vibration band and C–H bending (Ayad et al. 2017), respectively.

After the preparation of GO/DWCNTs/Oct- Fe_3O_4 /Cs, the characteristic peaks at 3441 , 1632 and 1442 cm^{-1} of Cs transferred to 3443 , 1635 and 1453 cm^{-1} respectively, indicating the linkage of Cs with Oct- Fe_3O_4 particles and GO/DWCNTs. These results are in agreement with those from earlier report about the interaction and linkage of Cs with Fe_3O_4 particles and GO. Likewise, the absorbance peak of Oct- Fe_3O_4 at 583 cm^{-1} shifted to 671 cm^{-1} , suggesting the Fe_3O_4 particles are linked successfully to Cs and GO/DWCNTs.

The Raman spectra of (a) GO, (b) DWCNTs, (c) Oct- Fe_3O_4 , (d) Cs and (e) GO/DWCNTs/Oct- Fe_3O_4 /Cs samples are shown in Fig. 3. Raman spectrum of GO sample

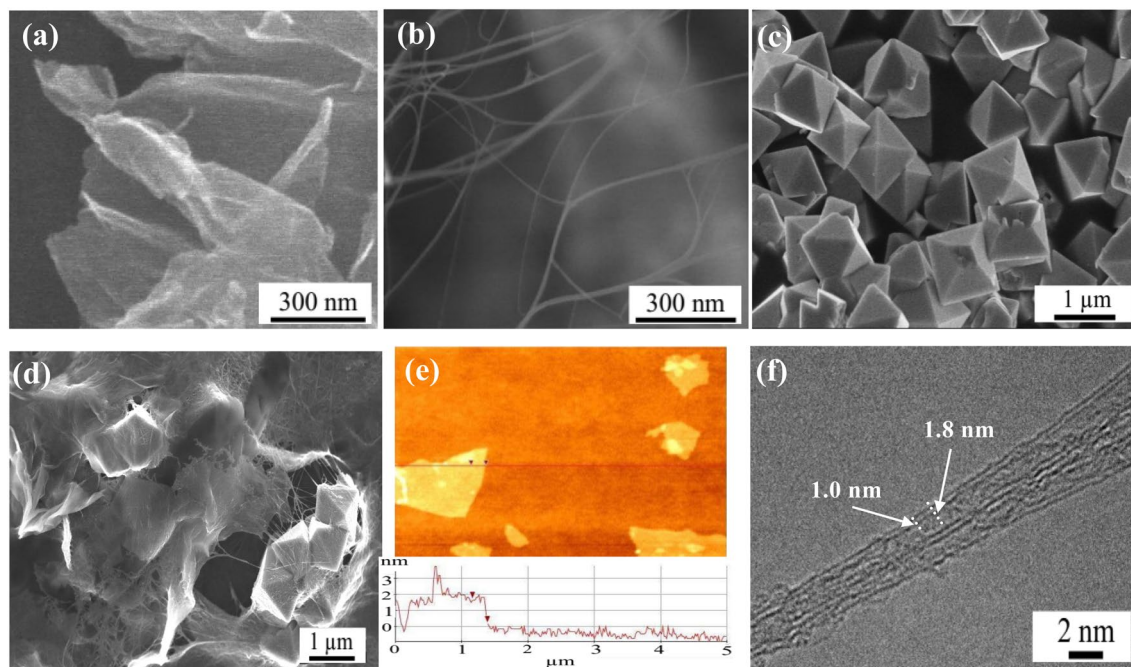


Fig. 1 SEM images of **a** GO, **b** DWCNTs, **c** Oct-Fe₃O₄ and **d** GO/DWCNTs/Oct-Fe₃O₄/Cs hybrid; **e** AFM image of GO and **f** TEM image of two DWCNT fibers

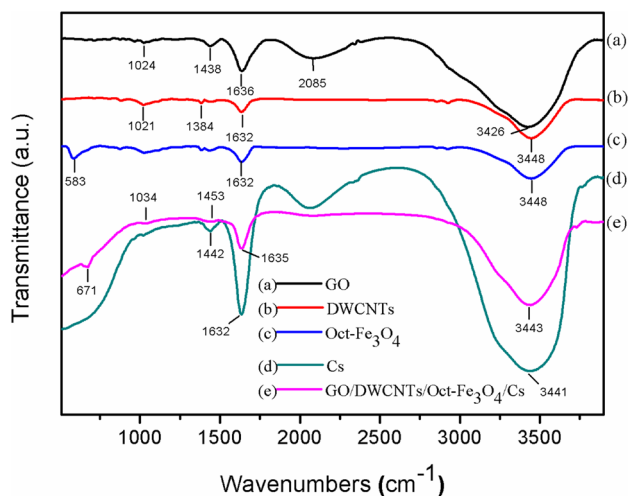


Fig. 2 FTIR spectra of (a) GO, (b) DWCNTs, (c) Oct-Fe₃O₄, (d) Cs and (e) GO/DWCNTs/Oct-Fe₃O₄/Cs

(Fig. 3a) exhibits the G band ($\sim 1602 \text{ cm}^{-1}$) and D band ($\sim 1338 \text{ cm}^{-1}$) which are ascribed to the vibrations of sp^2 carbon atom domains of graphite and the out-of-plane breathing mode of sp^2 atoms in graphite, respectively (Kumar et al. 2019). These two bands of DWCNTs (Fig. 3b) are located at 1590 cm^{-1} (G band) and 1326 cm^{-1} (D band). No Raman peak was observed for Oct-Fe₃O₄ (Fig. 3c) and Cs (Fig. 3d). For GO/DWCNTs/Oct-Fe₃O₄/Cs hybrid, the Raman spectrum showed a slight shift in

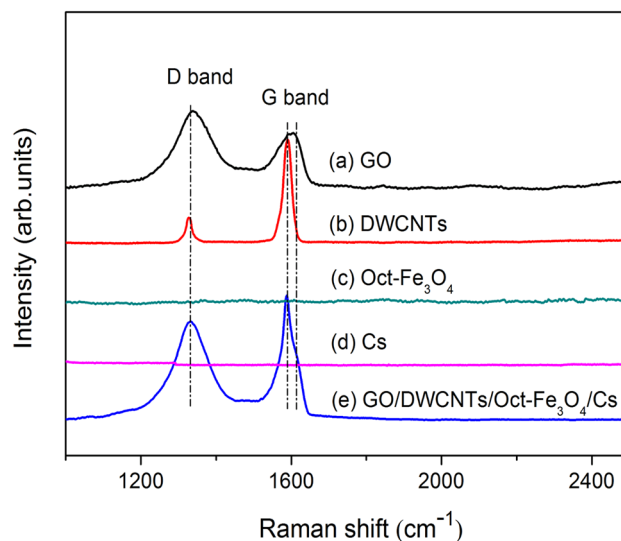


Fig. 3 Raman spectra of (a) GO, (b) DWCNTs, (c) Oct-Fe₃O₄, (d) Cs and (e) GO/DWCNTs/Oct-Fe₃O₄/Cs

the bands (D band at around 1332 cm^{-1} , G band at around 1589 cm^{-1} and a small peak at 1610 cm^{-1}). The intensity ratio between D and G bands (I_D/I_G) can be used to determine the defect density of graphite structure. The I_D/I_G of GO, GO/DWCNTs, and GO/DWCNTs/Oct-Fe₃O₄/Cs is ~ 1.4 , 0.21 , and 0.79 , respectively. These results indicate an interaction between GO and DWCNTs.

Figure 4 shows the CV responses of (a) bare SPAuE, (b) Oct-Fe₃O₄/Cs/SPAuE, (c) rGO/DWCNTs/Cs/SPAuE and (d) rGO/DWCNTs/Oct-Fe₃O₄/Cs/SPAuE in 2 mM [Fe(CN)₆]^{3-/4-}. The cyclic voltammogram of SPAuE showed a pair of redox peak with the peak-to-peak separation of 100 mV, and the peak current was about 10.7 μA. After modifying electrode surface with Oct-Fe₃O₄/Cs, rGO/DWCNTs/Cs and rGO/DWCNTs/Oct-Fe₃O₄/Cs, the peak current was 6.5 μA, 17.4 μA, 18.3 μA, respectively. It is obvious that the current response should be much improved in presence of highly conductive carbonaceous materials, but slightly decreased when there is only oxide particle on the electrode surface. However, the co-existence of these two materials

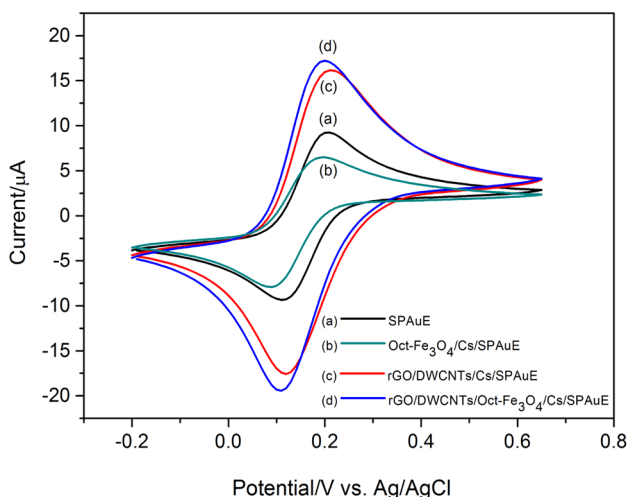


Fig. 4 Cyclic voltammograms of (a) bare SPAuE, (b) Oct-Fe₃O₄/Cs/SPAuE, (c) rGO/DWCNTs/Cs/SPAuE and (d) rGO/DWCNTs/Oct-Fe₃O₄/Cs/SPAuE in 2 mM [Fe(CN)₆]^{3-/4-} at a scan rate of 50 mV/s

must have inherited high conductivity of rGO/DWCNTs composite and good catalytic activity of oxide particles, so that the highest electrochemical responses were recorded on electrode modified with rGO/DWCNTs/Fe₃O₄/Cs. The electroactive surface area (*A_{app}*) of bare SPAuE, Oct-Fe₃O₄/Cs/SPAuE, rGO/DWCNTs/Cs/SPAuE and rGO/DWCNTs/Oct-Fe₃O₄/Cs/SPAuE (estimated from Randles–Sevcik equation) (Bard and Faulkner 2002) are 0.0341 cm², 0.0207 cm², 0.0554 cm² and 0.0583 cm², respectively. It is apparent that the effective area of rGO/DWCNTs/Oct-Fe₃O₄/Cs/SPAuE is the largest (1.7 times higher than that of bare SPAuE). The increase in electroactive surface area of rGO/DWCNTs/Oct-Fe₃O₄/Cs/SPAuE will facilitate the absorption of target analytes on the electrode surface and also provide more catalytic active sites, thus enhance the recorded electrochemical responses.

It is essential to optimize the substrate concentration (urea) in order to achieve good analytical performance of developed sensors. The hydrolysis of urea at different concentrations (5–50 mM) was recorded on SWV curves as shown in Fig. 5a. It was found that the current response was increased with increasing urea amount at concentrations less than 30 mM, but then decreased at higher urea concentrations (30–50 mM) (Fig. 5b). In deed, the substrate (urea) at too high concentration itself might exhibit inhibition towards catalytic activity of enzyme. Therefore, all sensing performances of as-prepared GLY sensors will be later performed in presence of 30 mM urea.

The sensing performance of GLY sensor based on rGO/DWCNTs/Oct-Fe₃O₄/Cs/SPAuE was evaluated at different concentrations of GLY (Fig. 6) using SWV technique. Obviously, the SWV peak currents were decreased in presence of inhibitor GLY (Fig. 6a). The higher concentration

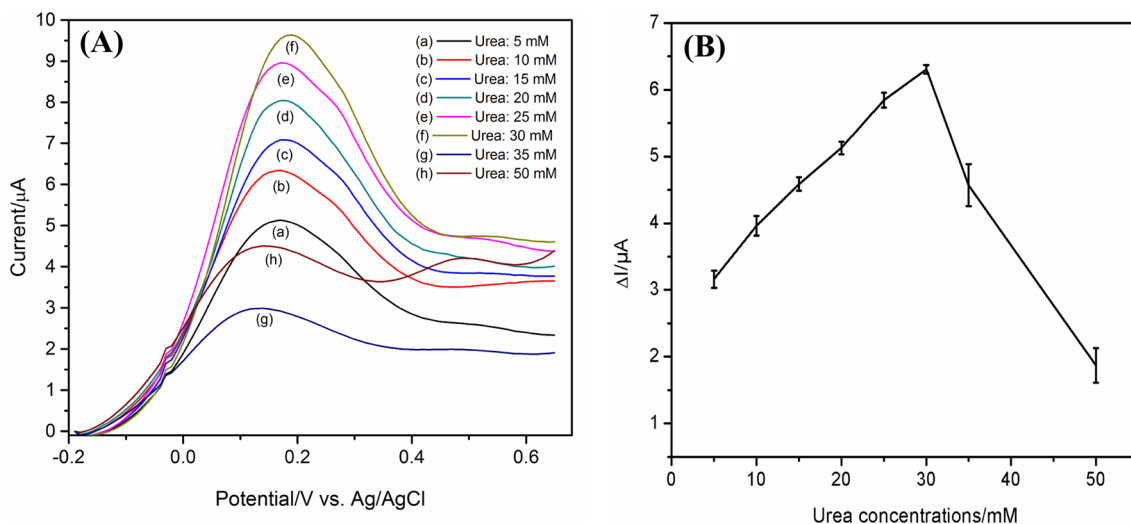


Fig. 5 a SWV and b output current responses of the fabricated sensor with urea concentration from 5 to 50 mM

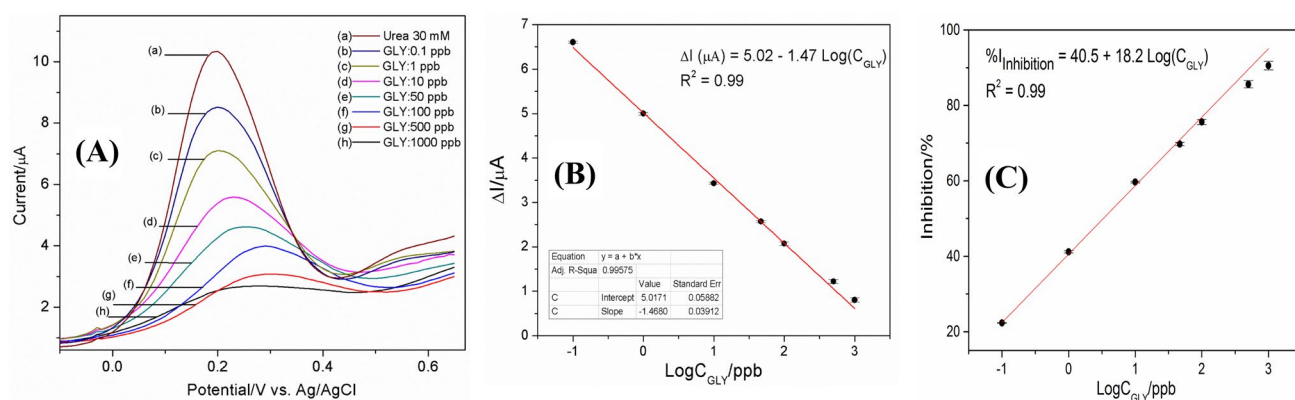


Fig. 6 **a** SWV, **b** current responses and **c** relationship between percentage inhibition of the fabricated sensor with GLY concentration from 0.1 to 1000 ppb

of GLY, the more the current decrease was obtained: ΔI (μA) = $5.02 - 1.47 \log C_{\text{GLY}}$ ($R^2 = 0.99$) (Fig. 6b). Consequently, the relative inhibition degree (RI) was found to be increased with GLY concentration: $\text{RI} (\%) = a + b \cdot \log C_{\text{GLY}}$ ($R^2 = 0.99$) (Fig. 6c). The limit of detection (LOD) was determined using the relationship $\text{LOD} = 3\sigma/S = 0.08$ ppb, where $\sigma = 0.03912$ was the standard deviation of the ordinate intercept and $S = 1.468$ was the analytical curve slope. This LOD value is much lower than the permissible value set by Environmental Protection Agency (EPA, 700 ppb) and World Health Organization (WHO, 900 ppb) in drinking water (Vaghela et al. 2018). Compared with previous reported works (Table S2 (Supporting information)), the developed sensor shows good sensitivity with a low LOD.

The reproducibility of the developed GLY sensors was tested on five different electrodes in the same manufacturing batch. The relative standard deviation (RSD) of the sensor at 100 ppb in urea solution is 2.14%. The stability of these sensors was also confirmed with the output signal was remained about 93% after a period of 30 days. The real sample analysis (Table 1) shows that the developed sensor was able to detect GLY at high recoveries (98.7%–106.9%). The results indicate that the proposed sensor is very promising for practical applications in determination of GLY in water environment.

In summary, rGO/DWCNTs/Oct- Fe_3O_4 /Cs hybrid structure was successfully prepared using a simple method. The as-synthesized material inherits high conductivity of three-dimensional carbonaceous structure and electro-catalytic activity of oxide particle. Consequently, the modification of electrode surface with this material helps to significantly improve electrochemical responses. GLY electrochemical sensor was then constructed by immobilizing directly urease enzyme onto electrode surface previously modified with as-prepared composite structure. The developed sensor exhibits good sensing performance with a large range of detection

Table 1 River water samples analysis

Sample	Added concentration (ppb)	Found concentration (ppb)	Recovery (%)	RSD (%)
River water 1	0.1	0.107	106.9	2.07
River water 2	100	98.7	98.7	2.12

0.1–1000 ppb, detection limit of 0.08 ppb and able to detect GLY in river water with high accuracy and good recovery.

Supplementary Information The online version contains supplementary material available at <https://doi.org/10.1007/s00128-021-03179-7>.

Acknowledgements This research is funded by Institute of Materials Science (IMS) under Grant Number CS.06/20-21 and supported by JSPS KAKENHI Grant Number JP17H03404 for Basic Research: Category B.

References

- Abe H, Naka T, Sato K et al (2019) Shape-controlled syntheses of magnetite microparticles and their magnetorheology. *Int J Mol Sci.* <https://doi.org/10.3390/ijms20153617>
- Ayad MM, Amer WA, Kotp MG et al (2017) Synthesis of silver-anchored polyaniline-chitosan magnetic nanocomposite: a smart system for catalysis. *RSC Adv.* <https://doi.org/10.1039/c7ra02575k>
- Bard AJ, Faulkner LR (2002) *Electrochemical methods: fundamentals and applications*, New York: Wiley, 2001, 2nd ed. *Russ J Electrochem.* <https://doi.org/10.1023/A:1021637209564>
- Bera M, Chandravati GP, Maji PK (2017) Facile one-pot synthesis of graphene oxide by sonication assisted mechanochemical approach and its surface chemistry. *J Nanosci Nanotechnol.* <https://doi.org/10.1166/jnn.2018.14306>

- Boikanyo D, Adekunle AS, Ebenso EE (2016) Electrochemical study of pyrene on glassy carbon electrode modified with metal-oxide nanoparticles and graphene oxide/multi-walled carbon nanotubes nanoplatfrom. *J Nano Res* 44:158–195
- Chen Q, Zheng J, Yang Q et al (2019) Insights into the glyphosate adsorption behavior and mechanism by a MnFe_2O_4 @cellulose-activated carbon magnetic hybrid. *ACS Appl Mater Interfaces*. <https://doi.org/10.1021/acsami.8b22386>
- Dağcı Kırışan K, Aksoy M, Topçu E (2018) Flexible and freestanding catalase- Fe_3O_4 /reduced graphene oxide paper: enzymatic hydrogen peroxide sensor applications. *Mater Res Bull*. <https://doi.org/10.1016/j.materresbull.2018.05.032>
- Duoc PND, Binh NH, Van HT et al (2020) A novel electrochemical sensor based on double-walled carbon nanotubes and graphene hybrid thin film for arsenic(V) detection. *J Hazard Mater*. <https://doi.org/10.1016/j.jhazmat.2020.123185>
- Ghalkhani M, Shahrokhian S, Navabi M (2020) Development of an electrochemical sensor based on (rGO-CNT) nanocomposite for raloxifene analysis. *Mater Chem Phys*. <https://doi.org/10.1016/j.matchemphys.2020.124131>
- Gholivand MB, Akbari A, Norouzi L (2018) Development of a novel hollow fiber-pencil graphite modified electrochemical sensor for the ultra-trace analysis of glyphosate. *Sens Actuators B*. <https://doi.org/10.1016/j.snb.2018.05.170>
- Hummers WS, Offeman RE (1958) Preparation of graphitic oxide. *J Am Chem Soc*. <https://doi.org/10.1021/ja01539a017>
- Hussain N, Das MR (2017) Magnetically recoverable graphene-based nanocomposite material as an efficient catalyst for the synthesis of propargylamines: via A3 coupling reaction. *New J Chem*. <https://doi.org/10.1039/c7nj03412a>
- Kumar R, Singh RK, Dubey PK et al (2015) Self-assembled hierarchical formation of conjugated 3D cobalt oxide nanobead-CNT-graphene nanostructure using microwaves for high-performance supercapacitor electrode. *ACS Appl Mater Interfaces*. <https://doi.org/10.1021/acsami.5b04336>
- Kumar R, Singh RK, Alaferdov AV, Moshkalev SA (2018) Rapid and controllable synthesis of Fe_3O_4 octahedral nanocrystals embedded-reduced graphene oxide using microwave irradiation for high performance lithium-ion batteries. *Electrochim Acta*. <https://doi.org/10.1016/j.electacta.2018.05.157>
- Kumar R, Joanni E, Savu R et al (2019) Fabrication and electrochemical evaluation of micro-supercapacitors prepared by direct laser writing on free-standing graphite oxide paper. *Energy*. <https://doi.org/10.1016/j.energy.2019.05.032>
- Motojyuku M, Saito T, Akieda K et al (2008) Determination of glyphosate, glyphosate metabolites, and glufosinate in human serum by gas chromatography–mass spectrometry. *J Chromatogr B*. <https://doi.org/10.1016/j.jchromb.2008.10.003>
- Nehru S, Sakthnathan S, Tamizhdurai P et al (2020) Reduced graphene oxide/multiwalled carbon nanotube composite decorated with Fe_3O_4 magnetic nanoparticles for electrochemical determination of hydrazine in environmental water. *J Nanosci Nanotechnol*. <https://doi.org/10.1166/jnn.2020.17379>
- Neves V, Heister E, Costa S et al (2012) Design of double-walled carbon nanotubes for biomedical applications. *Nanotechnology*. <https://doi.org/10.1088/0957-4484/23/36/365102>
- Pham VT, Cao TT, Le VC et al (2017) Effect of organic solvents on the properties of DWCNT/PEDOT:PSS transparent conductive films. *Mater Res Express*. <https://doi.org/10.1088/2053-1591/aa90ac>
- Sakthivel R, Annalakshmi M, Chen SM et al (2019) A novel sensitive and reliable electrochemical determination of palmitate based on CeO_2 /RGO/MWCNT ternary composite. *J Taiwan Inst Chem Eng*. <https://doi.org/10.1016/j.jtice.2018.11.008>
- Setznagl S, Cesarino I (2020) Copper nanoparticles and reduced graphene oxide modified a glassy carbon electrode for the determination of glyphosate in water samples. *Int J Environ Anal Chem*. <https://doi.org/10.1080/03067319.2020.1720667>
- Sok V, Fragoso A (2019) Amperometric biosensor for glyphosate based on the inhibition of tyrosinase conjugated to carbon nano-onions in a chitosan matrix on a screen-printed electrode. *Microchim Acta*. <https://doi.org/10.1007/s00604-019-3672-6>
- Turhan DÖ, Güngördü A, Özmen M (2020) Developmental and lethal effects of glyphosate and a glyphosate-based product on *Xenopus laevis* embryos and tadpoles. *Bull Environ Contam Toxicol*. <https://doi.org/10.1007/s00128-019-02774-z>
- Vaghela C, Kulkarni M, Haram S et al (2018) A novel inhibition based biosensor using urease nanoconjugate entrapped biocomposite membrane for potentiometric glyphosate detection. *Int J Biol Macromol*. <https://doi.org/10.1016/j.ijbiomac.2017.11.136>
- Wei X, Gao X, Zhao L et al (2013) Fast and interference-free determination of glyphosate and glufosinate residues through electrophoresis in disposable microfluidic chips. *J Chromatogr A*. <https://doi.org/10.1016/j.chroma.2013.01.039>
- Zhang Y, Dang Y, Lin X et al (2020) Determination of glyphosate and glufosinate in corn using multi-walled carbon nanotubes followed by ultra high performance liquid chromatography coupled with tandem mass spectrometry. *J Chromatogr A*. <https://doi.org/10.1016/j.chroma.2020.460939>
- Zhao Z, Zhang J, Wang W et al (2019) Synthesis and electrochemical properties of Co_3O_4 -rGO/CNTs composites towards highly sensitive nitrite detection. *Appl Surf Sci*. <https://doi.org/10.1016/j.apsusc.2019.04.202>

Publisher's note Springer Nature remains neutral with regard to jurisdictional claims in published maps and institutional affiliations.